Performance of a Five-Phase Induction Machine With Optimized Air Gap Field Under Open Loop *V/f* Control

César Cataldo Scharlau, Luís Fernando Alves Pereira, Luís Alberto Pereira, and Sérgio Haffner, *Member, IEEE*

***Abstract*—The paper assesses the steady-state performance of a five-phase induction machine fed by a modified open loop constant volt/hertz (*V/f*) control method, which imposes a trapezoidal induction waveform in the air gap under varying load conditions. The trapezoidal air gap induction is achieved through the imposition of an appropriate combination of the third harmonic and fundamental stator voltages. This harmonic combination is determined from the steady-state model using a mathematical optimization procedure, which allows to obtain the optimal weighting factors for each harmonic component. The optimized reference voltages lead to a trapezoidal air gap induction, which allows a better iron utilization and higher output torque for the same rms stator current when compared to sinusoidal air gap induction. The resulting air gap induction is obtained from the induced voltage of a full pitch search coil placed in the air gap. The proposed control scheme was successfully simulated and implemented on a five-phase prototype machine running under different load conditions. Experimental and simulations results show an increase in the torque/ampere relationship for loads above 50% when compared to the conventional *V/f* method using only the fundamental current and air gap induction. A comparison between the simulation and experimental curves presents a very good agreement that confirms and validates the parameters and model used.**

***Index Terms*—AC motor drives, induction machines, modeling, volt/hertz (*V/f*) control.**

NOMENCLATURE

v^s	Stator voltage.
$\overline{V}^s$	Phasor of stator voltage.
i^s	Stator current.
$\overline{I}^s$	Phasor of the stator current.
R^s	Stator resistance.
L^s	Stator inductance.
L^s_δ	Stator leakage inductance.
$\widehat{L}^{ss}_x$	Stator phase inductance for the x-harmonic component.
L^s_h	Main stator inductance.
$\overline{I}^{r\prime}$	Phasor of rotor current in stator reference frame.
R^r	Rotor resistance.
$R^{r\prime}$	Rotor resistance in stator reference frame.
L^r	Rotor inductance.
$L^{r\prime}_\delta$	Rotor leakage inductance in stator reference frame.
L^r_h	Main rotor inductance.
L^{sr}	Mutual inductance.
m_r	Number of rotor phases.
m_s	Number of stator phases.
q	number of stator slots per phase and pole.
ω_e	Rotor speed in electrical degrees.
ω_m	Rotor speed in mechanical degrees.
s	Rotor slip.
B	Flux density.
u	Induced voltage in the search coil.
γ	Angle between two stator slots.
μ_0	Permeability of air.
δ_e	Equivalent air gap.
N_s	Number of turns per stator coil.
θ	Stator coordinate in electrical degrees.
ℓ	Machine axial length.
D	Internal stator diameter.
R	Internal stator radius.
σ_p	Winding pitch.
p	Number of pole-pairs.
f_e	Reference frequency.
f_b	Base frequency.

Manuscript received October 30, 2007; revised March 26, 2008. Current version published November 21, 2008. Paper no. TEC-00384-2007.

C. C. Scharlau is with the Technology Faculty, National Industrial Training Service (SENAI), Porto Alegre 91140-000, Brazil (e-mail: cesarcs@gmail.com).

L. F. A. Pereira and L. A. Pereira are with the Electrical Engineering Department, Pontifical Catholic University of Rio Grande do Sul (PUCRS), Porto Alegre 90619-900, Brazil (e-mail: pereira@pucrs.br; lpereira@pucrs.br).

S. Haffner is with the Electrical Engineering Department, Santa Catarina State University (UDESC), Joinville 89223-100, Brazil (e-mail: haffner@ieee.org).

Digital Object Identifier 10.1109/TEC.2008.2001437

I. INTRODUCTION

THE INDUCTION machine has been widely used over the last two decades due to its robustness, versatility, and reliability. The development of solid-state inverters and control schemes has opened a range of applications for the induction machine in areas where dc machines were dominant. A widely used control technique for induction machines is the constant volt/hertz (*V/f*) method. The principle of *V/f* operation is well understood and commonly used in variable-speed drives [1].

In almost any kind of application, three-phase induction machines have been employed. The use of three-phase machines is based on long-established concepts where industrial power sources are three-phase systems. However, when the machine is not directly fed from the standard power sources, there is no need for a specified number of phases. In some cases, higher number of phases can be more appropriate and advantageous.

Many published papers have shown that five-phase machines have several advantages over conventional three-phase

ones [2]–[4]. One of these advantages is the fact that a five-phase induction machine can operate even when one phase is missing, as shown in [5]. This issue makes use of this kind of machine very attractive for applications that demand higher reliability such as electrical or hybrid vehicles, ship propulsion, and aerospace applications.

Nowadays, the known advantages of using multiphase induction motors can be effectively put into practice, as previous research has focused on the development, optimization, and application of multiphase machines [6]–[8]. Based on the additional freedom degree resulting from the high phase number, new space vector pulse width modulation (SVPWM) techniques have been recently presented and evaluated for the application to multiphase machine [9]. Moreover, drives based on a special series connection of two five-phase machines have also been investigated in [10]. It is shown that independent control of each machine is possible using a single current-controlled five-phase voltage source inverter as the supply.

The performance of induction machines with different number of phases for operation with static power converters is evaluated in [11]. This study concludes that machines with five phases can have a higher output torque/volume relationship as compared to conventional three-phase machines. In addition, the same study also showed that torque/volume relationship does not increase significantly when the phase number is increased above five.

One of the most important advantages of five-phase induction machines is the possibility of using the third-harmonic air gap flux density component to increase the output torque. The choice of an appropriate combination of the fundamental and the third-harmonic air gap flux density makes possible to obtain a trapezoidal induction waveform in the air gap. A trapezoidal flux density distribution improves the iron utilization leading to a higher power density and increased output torque.

In this paper, the performance of a five-phase machine with optimized air gap induction is evaluated through simulation and experimental results obtained from tests on a prototype machine. The machine is fed by a static PWM inverter employing an alternative *V/f* control strategy, which imposes a fundamental and a third-harmonic current to the stator phases. Choosing an appropriate combination of voltage components, a trapezoidal air gap induction under varying load conditions is achieved. The control strategy for five-phase induction machine is also presented and evaluated by simulation and experimental tests on a prototype machine. The developed control scheme is based on the traditional *V/f* technique in order to produce a third-harmonic component in the air gap flux density and in the stator current, aiming to improve the output torque. Although the weighted combinations of the fundamental and the third harmonic to improve the torque response had been already reported in preceding works [12]–[14], one of the main contributions of this paper is the determination of the weighting factors based on the electromagnetic model of a five-phase induction machine accounting for the effects of higher harmonics in the air gap field, fully described in [15].

The paper is organized as follows. First, the optimal relationship between the fundamental and third-harmonic components of air gap induction is determined based on the numerical solution of a mathematical optimization problem. After this, the amplitudes of the fundamental and third-harmonic current components are calculated from the reference fundamental and third-harmonic air gap induction using the steady-state machine model. In this part, it is also demonstrated that the harmonic content of the space distribution of the air gap induction and the harmonic content of the stator current are not the same. Considering that the control scheme is based on the *V/f* technique, the fundamental and third-harmonic current components are employed to obtain the fundamental and the third-harmonic reference voltages used for the five-phase induction motor control, resulting in the required flux density waveform in the air gap under different load conditions. The experimental setup allows the determination of the air gap induction from the induced voltage in a search coil placed in the air gap. Finally, the simulation and experimental results obtained with an induction machine prototype are presented and discussed.

II. Air Gap Flux Density

The main requirement on the control scheme is to keep the air gap induction waveform trapezoidal and independent of the machine load condition. Compared to a sinusoidal air gap waveform, this particular air gap induction waveform results in a better iron utilization as a larger portion of the backiron attains the same level of saturation. From this point of view, a rectangular waveform would be the ideal one; this waveform is not possible to achieve, in practice, using only the fundamental and the third-harmonic induction component. However, as shown in the next section, it is possible to find a combination of fundamental and third-harmonic induction that best approximates the ideal waveform. The mathematical description of the air gap induction is obtained from the electromagnetic model of five-phase induction machines described in [15]. In this model, the variables are first described by Fourier series, and then, transformed to symmetrical components of instantaneous value, as described in [16]. According to [15], the effect of the fundamental induction is linked to the first symmetrical component, while the third-harmonic induction component is linked to the third symmetrical component of the stator and rotor currents and voltages.

Considering the flux density produced in the air gap by one stator phase and disregarding saturation and field-distortion effects produced by stator and rotor slotting, the flux density under one pole at a given time can be approximated by Fig. 1. Thus, the mathematical expression of air gap flux density is

$$B(\theta,t)=\sum_{k=1}^{m_s} B_k(\theta,t) \tag{1}$$

where

$$B_k(\theta,t)=i_k^s(t)\sum_{n=1}^{\infty}\widehat{W}_n\sin(n\theta) \tag{2}$$

with the current of stator phase k given by

$$i_k^s(t)=\sum_{n=1}^{\infty}\widehat{I}_n\cos(n\omega_e t-\varphi_n) \tag{3}$$

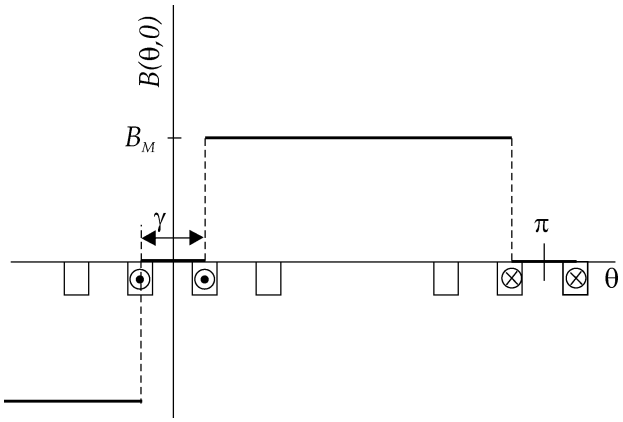

Fig. 1. Flux density in the air gap under one pole produced by one stator phase for a five-phase machine with two slots per phase and pole at time $t = 0$.

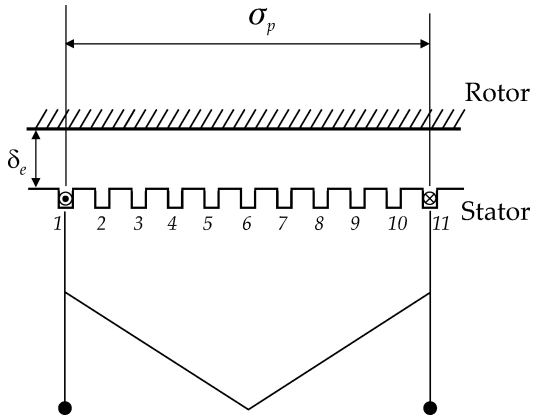

Fig. 2. Search coil with integral pitch.

and the factor $\widehat{W}_n$ defined as

$$\widehat{W}_n = \frac{4}{\pi}\frac{1}{n}\cos\left(\frac{n\gamma}{2}\right)\frac{\mu_0}{\delta_e}N_s. \tag{4}$$

The factor $\widehat{W}_n$ includes the effect of the winding distribution (winding factor) and the air gap effective permeance. Considering only the effects of the fundamental and the third-harmonic induction waves ($n = 1$ and $n = 3$), (1) can be rewritten as

$$B(\theta,t) = \widehat{B}_1\sin(\theta + \omega_e t - \varphi_1) + \widehat{B}_3\sin(3\theta + 3\omega_e t - \varphi_3) \tag{5}$$

with

$$\widehat{B}_1 = \frac{m_s}{2}\widehat{I}_1^s\widehat{W}_1 \tag{6}$$

and

$$\widehat{B}_3 = \frac{m_s}{2}\widehat{I}_3^s\widehat{W}_3. \tag{7}$$

In order to investigate the shape of the air gap induction, a search coil with integral pitch has been placed in the stator, as shown in Fig. 2. Considering that the machine has ten slot per pole, the first coil side is located in slot 1 and the other in slot 11. The resulting flux crossing the coil area was calculated considering two arbitrary positions for coil sides α and $\alpha + \pi$, according to (8), where α describes the position of the first coil side in the fixed stator reference frame

$$\phi(\alpha,t) = \int_{\alpha}^{\alpha+\pi}\frac{\ell R}{p}B(\theta,t)d\theta. \tag{8}$$

By substituting (5) in (8), the flux equation can be rewritten as

$$\phi(\alpha,t) = \frac{\ell R}{p}\int_{\alpha}^{\alpha+\pi}[\widehat{B}_1\sin(\theta + \omega_e t - \varphi_1) + \widehat{B}_3\sin(3\theta + 3\omega_e t - \varphi_3)]d\theta. \tag{9}$$

Evaluating the integral in expression (9) yields

$$\phi(\alpha,t) = \frac{-2\ell R}{p}[\widehat{B}_1\cos(\alpha + \omega_e t - \varphi_1) + \frac{\widehat{B}_3}{3}\cos(3\alpha + 3\omega_e t - \varphi_3)]. \tag{10}$$

The induced voltage at the search coil terminals is given by the time derivative of (10) as

$$u(\alpha,t) = -\frac{d\phi(\alpha,t)}{dt}$$
$$u(\alpha,t) = \frac{2\omega_e\ell R}{p}[\widehat{B}_1\sin(\alpha + \omega_e t - \varphi_1) + \widehat{B}_3\sin(3\alpha + 3\omega_e t - \varphi_3)]. \tag{11}$$

Comparing (5) and (11), it is possible to conclude that the induced voltage measured at the terminals of search coil presents the same shape as the induction produced in the air gap by the fundamental and third-harmonic currents. They differ only by a multiplying factor as the term in brackets is equal to (5). Therefore, the time distribution of the induced voltage $u(\alpha,t)$ corresponds exactly to the spatial induction distribution $B(\theta,t)$. This correspondence can be better understood by considering an arbitrary instant of time, for example, $t = 0$, and an arbitrary stator position, for example, $\alpha = 0$, in (5) and (11) as

$$B(\theta,0) = \widehat{B}_1\sin(\theta - \varphi_1) + \widehat{B}_3\sin(3\theta - \varphi_3) \tag{12}$$

$$u(0,t) = K_u[\widehat{B}_1\sin(\omega_e t - \varphi_1) + \widehat{B}_3\sin(3\omega_e t - \varphi_3)] \tag{13}$$

with

$$K_u = \frac{2\omega_e\ell R}{p} = \frac{\omega_e\ell D}{p}. \tag{14}$$

It must be pointed out that (5) and (13) have the same shape, differing from each other only by the amplitude factor K_u. Besides, $B(\theta,t)$ represents a rotating wave with a fixed pattern and rotational speed ω_e at any time instant. For brevity, in the rest of the paper, the induction $B(\theta,t)$ will be referred to as $B(\theta)$, while the induced voltage $u(\alpha,t)$ as $u(t)$.

The induced voltage given by (11) takes into account only the stator currents for no-load condition case. When the machine is under load, the resulting field in the air gap is produced by the stator and rotor currents. The effect of the rotor currents on the field in the air gap can be considered multiplying the stator

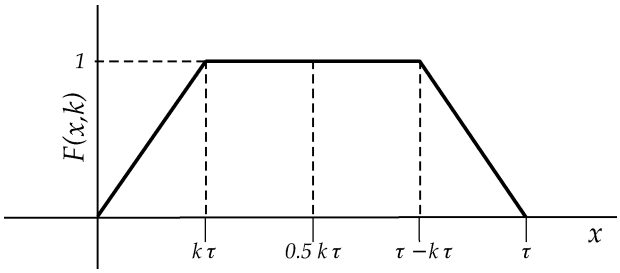

Fig. 3. Division of the trapezoidal waveform into four sections.

currents by the following complex factors:

$$\overline{K}_1^r = 1 - \frac{m_r}{2}\frac{m_s}{2}\frac{(L_1^{sr})^2}{L_1^s}\frac{j\omega_e}{[(R_1^r/S) + j\omega_e L_1^r]} \tag{15}$$

$$\overline{K}_1^r = \widehat{K}_1^r \angle\varphi_{k1} \tag{16}$$

$$\overline{K}_3^r = 1 - \frac{m_r}{2}\frac{m_s}{2}\frac{(L_3^{sr})^2}{L_3^s}\frac{j3\omega_e}{[(R_3^r/S) + j3\omega_e L_3^r]} \tag{17}$$

$$\overline{K}_3^r = \widehat{K}_3^r \angle\varphi_{k3}. \tag{18}$$

In this way, the steady-state expression of induced voltage in the search coil considering the rotor current is given by

$$u(t) = K_u[\widehat{B}_1\widehat{K}_1^r \sin(\omega_e t - \varphi_1 + \varphi_{k1}) + \widehat{B}_3\widehat{K}_3^r \sin(3\omega_e t - \varphi_3 + \varphi_{k3})]. \tag{19}$$

III. *V/f* Control for Five-Phase Induction Motors

The control for five-phase induction motors developed in this paper aims to impose an optimized trapezoidal waveform flux density in air gap, improving the iron utilization and increasing the output torque. This objective is achieved by using the steady-state model of the induction machine and validated through the induced voltage in a search coil placed in the air gap. Based on the machine equations, it is possible to calculate the relative magnitude of the fundamental and the third-harmonic stator voltages to obtain the required induction waveform.

A. Stator Current Design

Using only the fundamental and the third-harmonic induction waves, it is not possible to achieve an ideal rectangular waveform for the induction in the air gap. However, a trapezoidal waveform can be designed using the steady-state model of the fundamental and third-harmonic air gap induction, which is similar to a rectangular waveform. A trapezoidal waveform is considered better than a sine wave in terms of torque production and iron utilization, as a larger portion of the iron attains the maximum induction value at the same time.

For the sake of analysis and current design practice, the required trapezoidal wave was divided into four sections, as seen in Fig. 3. The shape of the curve is defined by the free parameter k and the corresponding Fourier series is given in the sequel

$$F(x,k) = \sum_{i=0}^{\infty} \alpha_i(k) \sin\left(i\frac{\pi x}{\tau}\right) \tag{20}$$

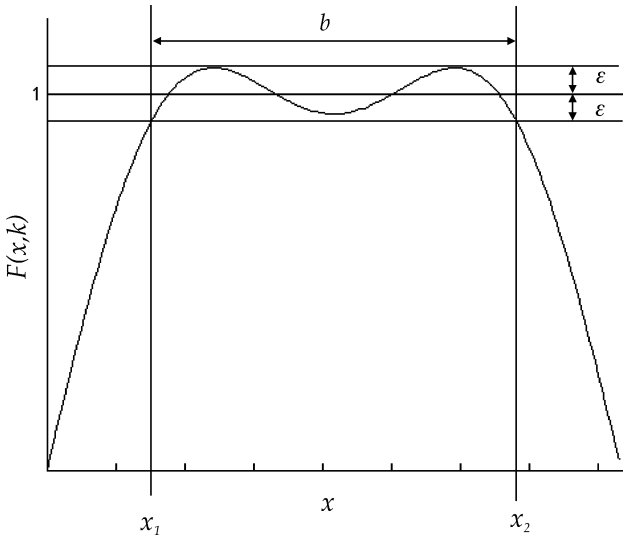

Fig. 4. Width of the flat portion b of the trapezoidal waveform curve depending on the amplitude of the oscillation levels ε.

where

$$\alpha_i(k) = \frac{4}{\pi i}\frac{\sin(k\pi i)}{k\pi i}, \qquad i = 1, 3, 5, \ldots \tag{21}$$

Considering only two terms (fundamental and third-harmonic components), (20) can be rewritten as

$$F(x,k) = \alpha_1(k)\sin\left(\frac{\pi x}{\tau}\right) + \alpha_3(k)\sin\left(3\frac{\pi x}{\tau}\right). \tag{22}$$

An optimal combination of the coefficients $\alpha_1(k)$ and $\alpha_3(k)$ can be determined through a formal optimization procedure, resulting in values for the coefficients that best approximate the desired waveform. The optimization problem consists of obtaining a quasi-trapezoidal waveform with the largest flat portion, resulting in the following expression

$$\max_k b = |x_1 - x_2| \tag{23}$$

subject to $|1 - F(x,k)| < \varepsilon \;\forall\; x \in [x_1; x_2]$, where ε is a design factor defined so as to reduce the oscillation of the flat level and b is the width of the flat part of the wave, as shown in Fig. 4. Choosing $\varepsilon = 0.005$, the solution of the optimization problem indicates that the wave with the largest flat portion is obtained for $k = 0.1157$. This condition yields $\alpha_1 = 1.1587$ and $\alpha_3 = 0.1588$ ($\alpha_3/\alpha_1 = 0.137$). However, the practical implementation and experimental results obtained by using this relationship led to undesired oscillations of the flat portion of the air gap induction. Therefore, in order to minimize the oscillations, the design factor ε had to be further reduced and the optimization procedure repeated resulting in $\alpha_3/\alpha_1 = 0.107$. This relationship proved to be better, considering the practical implementation and the approximations introduced in the model as it results in an air gap induction with a flat portion and no oscillation. Thus, $\alpha_3/\alpha_1 = 0.107$ was used for the experimental tests presented in Section V.

To achieve the required trapezoidal induction waveform in the air gap, an appropriate combination for the fundamental and the third-harmonic induction amplitudes, $\widehat{B}_1$ and $\widehat{B}_3$, must

be found. This optimized combination can be obtained from a comparison of (5) and (22) as described next.

According to (6), $\widehat{B}_1$ is proportional to $\widehat{I}_1^s$ and $\widehat{W}_1$, while according to (7), $\widehat{B}_3$ is proportional to $\widehat{I}_3^s$ and $\widehat{W}_3$. Considering that (4) implies different values for $\widehat{W}_1$ and $\widehat{W}_3$, it is noticeable that to obtain a trapezoidal flux density in the air gap under one pole, the stator currents cannot have the same shape as the air gap induction wave.

The amplitude of the fundamental and the third-harmonic stator currents that must be imposed to obtain the trapezoidal waveform can be calculated using (24) and (25). These equations are obtained by comparison of (19) and (22) for the no-load condition case ($\widehat{K}_1^r = 1$ and $\widehat{K}_3^r = 1$)

$$\widehat{I}_{1\ \mathrm{ref}}^s = I_{1\ \mathrm{ref}}^s \sqrt{2} = \frac{2\widehat{B}_1}{m_s \widehat{W}_1} \tag{24}$$

$$\widehat{I}_{3\ \mathrm{ref}}^s = I_{3\ \mathrm{ref}}^s \sqrt{2} = \frac{2\widehat{B}_3}{m_s \widehat{W}_3}. \tag{25}$$

Thus, for a given relationship $\widehat{B}_3/\widehat{B}_1$, the corresponding relationship between the currents $\widehat{I}_3$ and $\widehat{I}_1$ is

$$\frac{\widehat{I}_3}{\widehat{I}_1} = \frac{\widehat{W}_1 \widehat{B}_3}{\widehat{W}_3 \widehat{B}_1}. \tag{26}$$

It can be seen from (26) that the relative amplitude between the third harmonic and fundamental currents is different from the relative amplitude between the fundamental and third-harmonic induction waves.

In order to assess the influence of the relationship between the fundamental and the third-harmonic stator current components on the induction waveform, several simulations have been performed using [6], [7], and [19]. For a five-phase machine, with $q = 2$ and full pitch winding, the relationship between $\widehat{W}_3$ and $\widehat{W}_1$ is $\widehat{W}_3 \approx 1/3\widehat{W}_1$, resulting in

$$\frac{\widehat{I}_3}{\widehat{I}_1} \approx 3\frac{\widehat{B}_3}{\widehat{B}_1}. \tag{27}$$

This fact is illustrated in Fig. 5, where the third-harmonic current amplitude is 40% of the fundamental wave, while the corresponding third-harmonic induction wave is 14% of the fundamental wave.

B. Stator Reference Voltage Design

In the proposed *V/f* control scheme, stator voltages are imposed based on reference values for the voltages. The reference voltages have to be determined in such a way that at steady state, the required currents flow in the machine. The fundamental and third-harmonic stator reference voltages are obtained using the steady-state model of a five-phase induction machine. This task can be performed using the corresponding equivalent circuits for each harmonic component, both shown in Fig. 6. It should be noticed that both circuits are completely independent from each other.

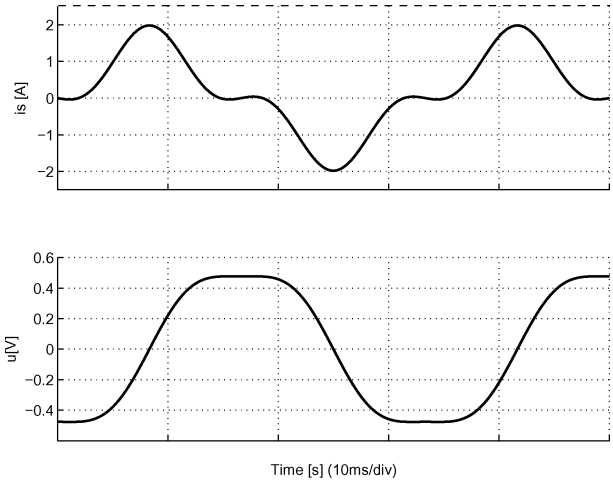

Fig. 5. Stator current and corresponding air gap induction.

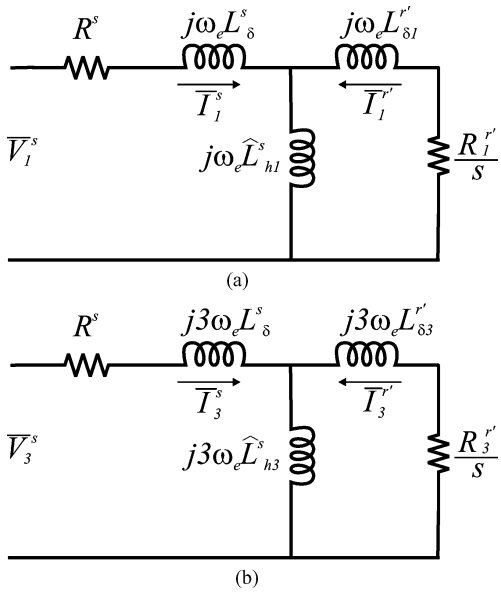

Fig. 6. Steady-state equivalent circuits of five-phase induction machine. (a) Fundamental. (b) Third harmonic.

From the equivalent circuit of the fundamental [see Fig. 6(a)], the following voltage equations result:

$$\overline{V}_1^s = R^s \overline{I}_1^s + j\omega_e L_\delta^s \overline{I}_1^s + j\omega_e \widehat{L}_{h1}^s (\overline{I}_1^{r\prime} + \overline{I}_1^s) \tag{28}$$

$$0 = \frac{R_1^{r\prime}}{s} \overline{I}_1^{r\prime} + j\omega_e L_{\delta 1}^{r\prime} \overline{I}_1^{r\prime} + j\omega_e \widehat{L}_{h1}^s (\overline{I}_1^{r\prime} + \overline{I}_1^s) \tag{29}$$

where

$$R_1^{r\prime} = R_1^r \frac{\widehat{L}_{h1}^s}{\widehat{L}_h^r} \tag{30}$$

$$L_{\delta 1}^{r\prime} = L_{\delta 1}^r \frac{\widehat{L}_{h1}^s}{\widehat{L}_h^r} \tag{31}$$

$$\widehat{L}_h^r = L_h^r \frac{m_r}{m_r - 1} \tag{32}$$

$$\widehat{L}_{h1}^s = \frac{m_s}{2} \widehat{L}_1^{ss}. \tag{33}$$

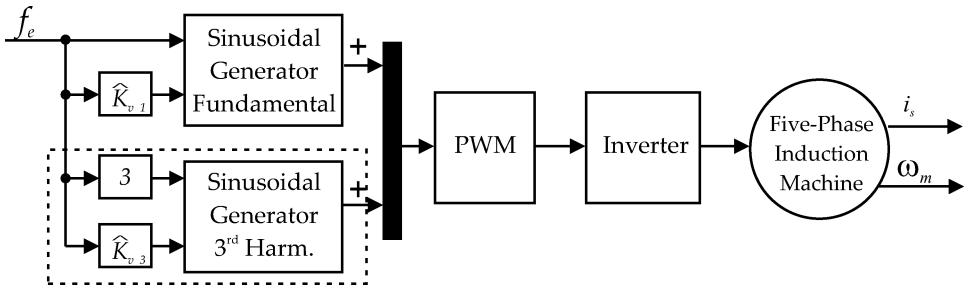

Fig. 7. Block diagram of control scheme.

A similar set of equations can be derived from the equivalent circuit of the third harmonic [see Fig. 6(b)]:

$$\overline{V}_3^s = R^s \overline{I}_3^s + j3\omega_e L_\delta^s \overline{I}_3^s + j3\omega_e \widehat{L}_{h3}^s (\overline{I}_3^{r\prime} + \overline{I}_3^s) \quad (34)$$

$$0 = \frac{R_3^{r\prime}}{S}\overline{I}_3^{r\prime} + j3\omega_e L_{\delta 3}^{r\prime}\overline{I}_3^{r\prime} + j3\omega_e \widehat{L}_{h3}^s (\overline{I}_3^{r\prime} + \overline{I}_3^s) \quad (35)$$

where

$$R_3^{r\prime} = R_3^r \frac{\widehat{L}_{h3}^s}{\widehat{L}_h^r} \quad (36)$$

$$L_{\delta 3}^{r\prime} = L_{\delta 3}^r \frac{\widehat{L}_{h3}^s}{\widehat{L}_h^r} \quad (37)$$

$$\widehat{L}_{h3}^s = \frac{m_s}{2}\widehat{L}_3^{ss}. \quad (38)$$

Using (28) and (34), the reference voltage at rated frequency and no-load condition ($\overline{I}_1^{r\prime} = 0$ and $\overline{I}_3^{r\prime} = 0$) can be stated as

$$V_{1\,\mathrm{ref}}^s = I_{1\,\mathrm{ref}}^s |R^s + j\omega_e L_\delta^s + j\omega_e \widehat{L}_{h1}^s| \quad (39)$$

$$V_{3\,\mathrm{ref}}^s = I_{3\,\mathrm{ref}}^s |R^s + j3\omega_e L_\delta^s + j3\omega_e \widehat{L}_{h3}^s|. \quad (40)$$

C. Proposed Control Scheme

Fig. 7 shows a schematic diagram of the control scheme. The structure is similar to the open-loop constant *V/f* method, where a new block has been added (dashed line). This new block generates voltage references for the third-harmonic voltage component using f_e as the reference frequency. The magnitudes of the reference voltages are dictated by the constants $\widehat{K}_{v1}$ and $\widehat{K}_{v3}$, calculated from (39) and (40), as

$$\widehat{K}_{v1} = \frac{V_{1\,\mathrm{ref}}^s \sqrt{2}}{f_b} \quad (41)$$

$$\widehat{K}_{v3} = \frac{V_{3\,\mathrm{ref}}^s \sqrt{2}}{f_b} \quad (42)$$

where f_b is the base frequency.

IV. Experimental Setup

In order to validate and evaluate the performance of the control scheme, a test bed was implemented and tested on a five-phase prototype machine built in the frame of a 3/4 HP induction motor of 220 V. The basic data of this machine are listed in Table I and the main parameters are shown in Table II. All the parameters used for the simulation were determined from the machine data and according to [15]. During the tests, the air gap induction was measured using the induced voltage in the search coil with integral pitch. The search coil sides are located in the air gap in the middle of a slot opening. In this way, the signal produced by this coil has the same waveform as the resulting air gap induction.

Fig. 8 shows the block diagram of the hardware used to obtain the results. The Matlab/Simulink program is installed on the personal computer together with the respective packages for real time, simulation, and control. Signals coming from the machine, such as rotor speed, stator currents, stator voltages, and the induced voltage at the search coil terminals are acquired through a specific data-acquisition board. The five-phase inverter is implemented using two three-phase inverters. The PWM method

TABLE I
PROTOTYPE DATA

Data	Value
external stator diameter	130.3 mm
internal stator diameter (D)	80.0 mm
axial length (ℓ)	64.0 mm
equivalent air gap length (δ_e)	0.48 mm
winding pitch (σ_p)	10 slots
number of turns per stator coil (N_s)	90
number of slots in stator	40
number of slots in rotor	30
number of pole-pairs (p)	2

TABLE II
PROTOTYPE PARAMETERS

Parameter	Value	Parameter	Value
R^s	3.48 Ω	L_δ^s	4 mH
L_h^r	0.79 μH	L_h^s	74.5 mH
R_1^r	8.10 μΩ	R_3^r	42.50 μΩ
$L_{\delta 1}^r$	0.033 μH	$L_{\delta 3}^r$	0.154 μH
$\widehat{L}_1^{ss}$	151.0 μH	$\widehat{L}_3^{ss}$	18.4 μH
L_1^s	168.9 mH	L_3^s	21.0 mH
L_1^r	0.71 μH	L_3^r	0.92 μH
L_1^{sr}	76.4 μH	L_3^{sr}	21.9 μH

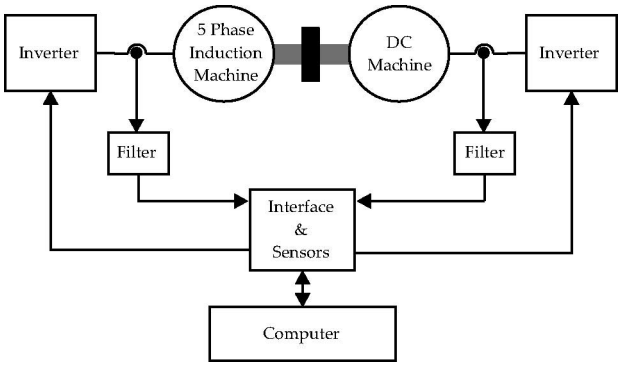

Fig. 8. Experimental setup used to evaluate the performance of the proposed control scheme.

used in the tests is the carrier-based PWM with switching frequency of 20 kHz. Second-order low-pass filters are used to perform the current and voltage measurements. The experimental setup has also a programmable load consisting of a dc motor operating in four quadrants.

V. Simulation and Experimental Results

Prior to the experimental tests, several simulations have been performed using built-in toolboxes available in Matlab/Simulink. Furthermore, additional blocks with the mathematical models of the experimental setup components were used for the simulation.

The first set of tests was carried out to validate the phase relationship of the third-harmonic and fundamental component of the stator current regarding the production of a trapezoidal induction waveform in the air gap. These tests also allowed to evaluate the accuracy of the machine parameters used in the model as they include practical approximation factors concerning saturation and slotting effects. These factors introduce a correction in the values of the inductances in order to account for the iron saturation and magnetic field distortion caused by the presence of slots (Carter factor). The relationship between fundamental and third-harmonic induction components used is $\alpha_3/\alpha_1 = 0.107$, which was determined by applying the optimization process described in Section III-A.

Figs. 9–11 show the stator current and air gap induction under three different load conditions, where the following factors have been used for all cases: $f_b = 60$ Hz, $\widehat{K}_{v1} = 1.278$ V/Hz, and $\widehat{K}_{v3} = 0.229$ V/Hz, f_b being the base frequency.

Fig. 9 refers to the no-load condition. In Fig. 9(a), the imposed phase-to-neutral stator voltage is plotted, and in Fig. 9(b), the stator current waveform is shown. With the given harmonic voltage combination, the air gap induction attains the required waveform, as it can be seen in Fig. 9(c). It must be pointed out that the harmonic content of the voltage, current, and air gap induction are different, as presented in Table III. This difference can be better understood, considering the fact that the resulting air gap induction is produced by currents flowing in all five phases. Besides, according to (2), the air gap induction is influenced by the way the windings are distributed in the stator slots, as described in Section II. Therefore, the current and air gap induction will have different waveforms. The difference between current and voltage waveforms can be explained, considering that (39) and (40) define a different relation between fundamental and the third harmonic for the voltage in comparison to the same relation for the current components. For the no-load case, the phase difference between the fundamental and the third-harmonic current is about 180°, while the phase difference in the air gap induction and the stator voltage is near to zero. In the limit case with no slip ($s = 0$), the phase difference of the

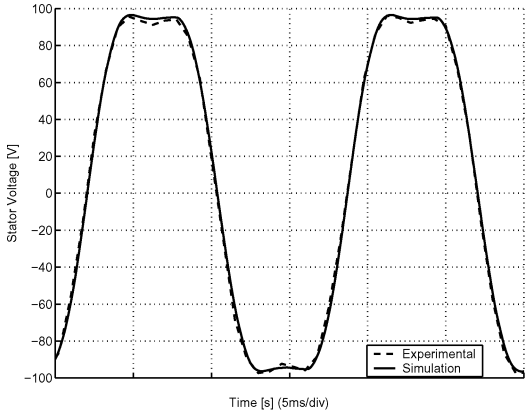

(a)

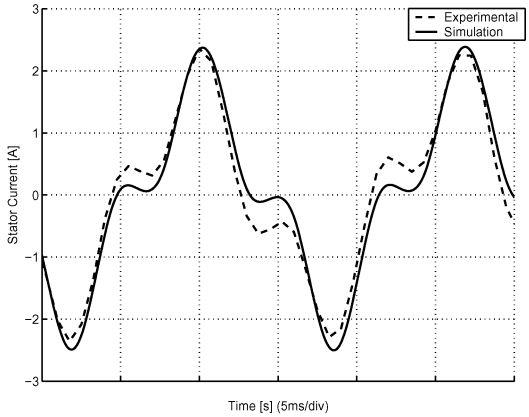

(b)

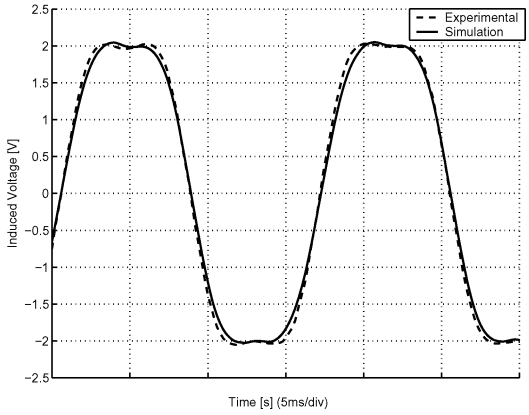

(c)

Fig. 9. Simulation and experimental results of the control scheme with no load. (a) Stator voltage. (b) Stator current. (c) Induced voltage.

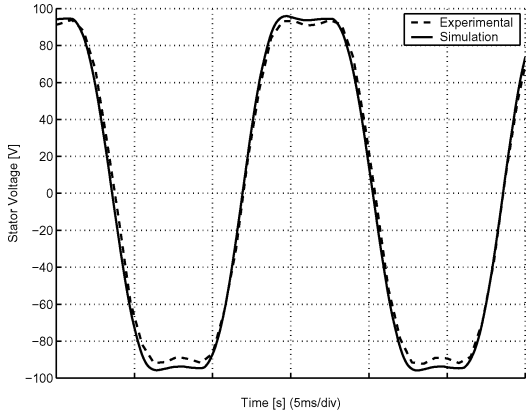

(a)

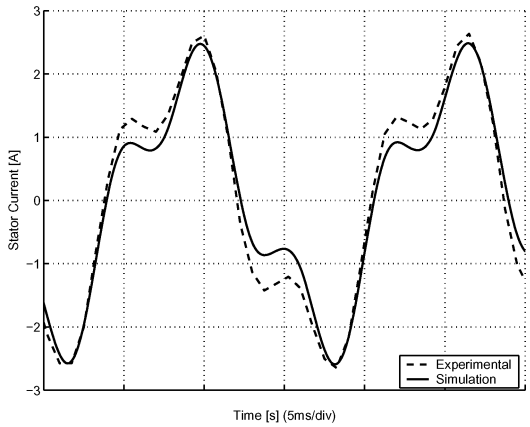

(b)

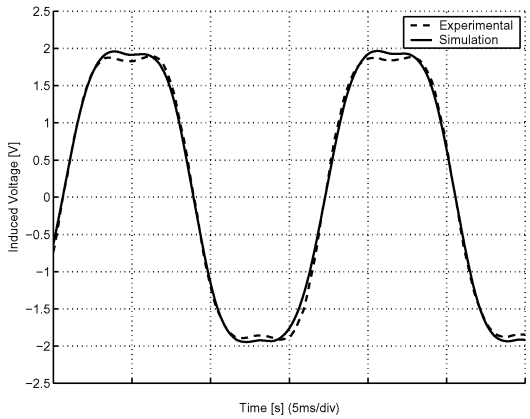

(c)

Fig. 10. Simulation and experimental results of the control scheme with 1 Nm load. (a) Stator voltage. (b) Stator current. (c) Induced voltage.

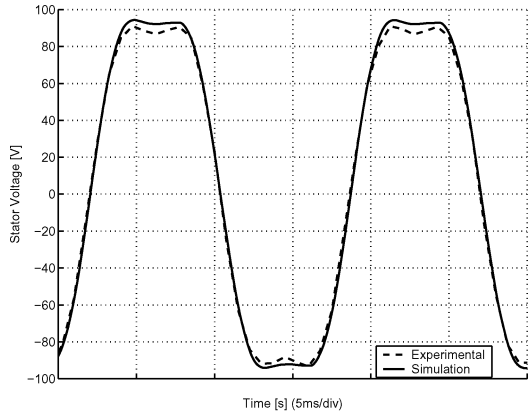

(a)

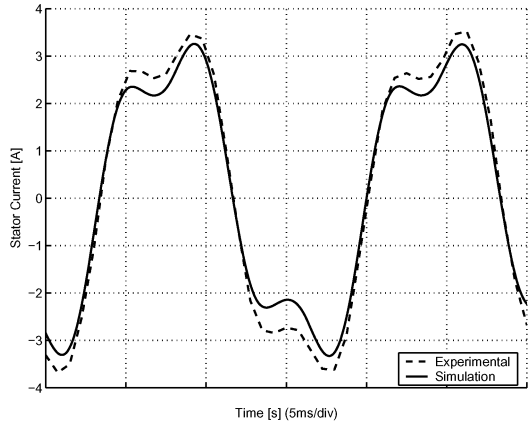

(b)

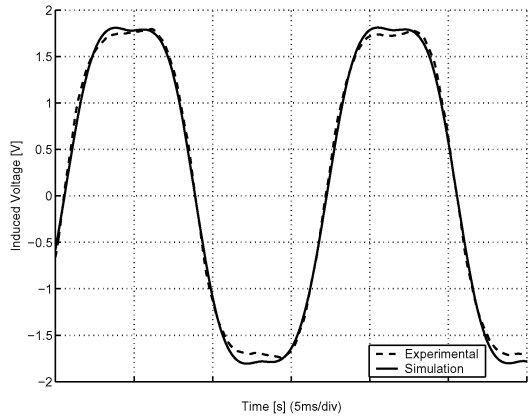

(c)

Fig. 11. Simulation and experimental results of the control scheme with 2.7 Nm load. (a) Stator voltage. (b) Stator current. (c) Induced voltage.

current components would tend to 180°. Comparing the simulated curves with the experimental curves, a good agreement between them could be observed, especially in the induced voltage in the search coil. The differences in the simulated and measured currents are introduced by the effects not entirely included in the model, such as slotting and saturation effects. These factors affect basically the values of the inductances in a form very difficult to determine using analytical methods.

The imposed stator voltage should result in a trapezoidal air gap induction with about 10.7% of the third-harmonic content. The experimental results show a relation very close to this value in practically all load conditions (10%) as can be seen in the corresponding columns in Table III.

Similar tests have been carried out with load torques ranging from 1 Nm (40% of rated torque) to 2.7 Nm (100% of the rated torque). The experimental and simulated results for the case of 1.0 Nm are shown in Fig. 10 and Table III. Applying the same

TABLE III
HARMONIC COMPONENTS

Load	Simulation							Experimental						
	I^s		u		V^s		Phase	I^s		u		V^s		Phase
[N.m]	Fund.	3^{rd} H.	Fund.	3^{rd} H.	Fund.	3^{rd} H.		Fund.	3^{rd} H.	Fund.	3^{rd} H.	Fund.	3^{rd} H.	
0	100%	37%	100%	12%	100%	14%	170	100%	44%	100%	10%	100%	16%	149
1.0	100%	34%	100%	12%	100%	14%	84	100%	35%	100%	10%	100%	16%	63
2.0	100%	29%	100%	12%	100%	14%	71	100%	27%	100%	10%	100%	16%	58
2.7	100%	26%	100%	12%	100%	14%	49	100%	22%	100%	10%	100%	16%	25

TABLE IV
EXPERIMENTAL RESULTS

Load	I^s $[A]$ (rms)			u $[V]$ (rms)			ω_m [rpm]			s [%]		
[N.m]	Conv.	Prop.	Dif.	Conv.	Prop.	Dif.	Conv.	Prop.	Dif.	Conv.	Prop.	Dif.
0	1.10	1.31	+20%	1.484	1.686	+14%	1790	1795	+0.3%	0.56	0.28	-50%
1	1.55	1.67	+8%	1.370	1.562	+14%	1734	1750	+0.9%	3.67	2.78	-24%
2	2.34	2.25	-4%	1.262	1.474	+17%	1662	1702	+2.4%	7.67	5.44	-29%
2.7	2.90	2.70	-7%	1.206	1.444	+20%	1608	1668	+3.7%	10.67	7.33	-31%

Conv. - Conventional method. Prop. - Proposed method. Dif - Difference

voltage as in the no-load case, a trapezoidal induction waveform is produced in the air gap. However, the current waveform changed. Comparing Figs. 9(b) and 10(b), it can be observed that the phase difference between the harmonic components has also changed. The results for 2.7 Nm are presented in Fig. 11 and Table III. The applied voltage, as given by (39) and (40), has not been changed. It can be observed that for all load conditions, the resulting air gap induction was kept trapezoidal as required. On the other hand, the stator current waveform changes significantly. This change can be explained considering that the equivalent circuit of each harmonic has a different input impedance. These impedances change with the load condition in a different way, resulting in a different waveform for the current for each load condition. The change in the current can also be explained by considering that the resulting field in the air gap under load is produced not only by the stator current but also by the rotor currents, as stated by (15)–(19). The air gap field is produced by the composition of the rotor and stator field, each one produced by its corresponding current. Thus, the relationship between stator and rotor currents change with the load condition in order to maintain the same air gap induction waveform. In this way, the desired trapezoidal air gap induction is produced by stator currents having a waveform different from a trapezoidal. The results for the loaded machine also show that the simulated and measured curves agree very well.

In order to make a comparison of the developed control scheme with the conventional *V/f* control method employing only the fundamental voltage, several tests have been performed with $\widehat{K}_{v3} = 0$ V/Hz and $\widehat{K}_{v1} = 1.137$ V/Hz. For these tests, the machine was fed with a pure sinusoidal voltage, with $f_b =$ 60 Hz, producing a sinusoidal air gap induction. In addition, the factor $\widehat{K}_{v1}$ was adjusted so that the peak air gap induction achieves the same value as in the proposed control scheme. The measured induced voltage is shown in Fig. 12.

Table IV summarizes the experimental results of both control techniques for different load conditions. For light-load condition (less than 50%), the rms value of the current for the developed control scheme is higher than the rms current with only the fundamental present (conventional *V/f* method). At no load, an

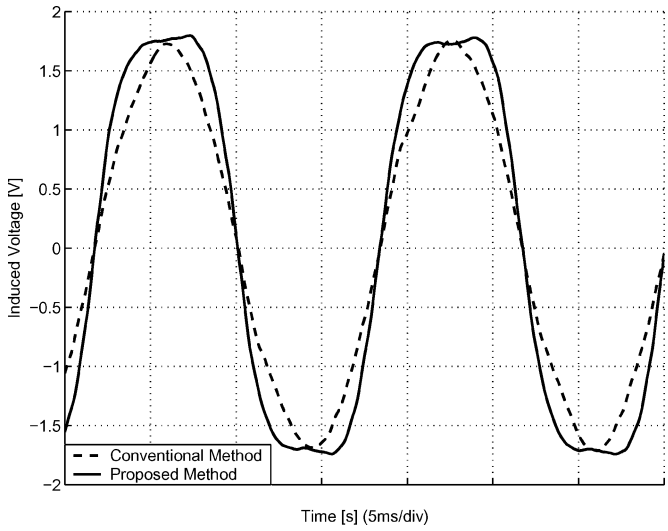

Fig. 12. Measured induced voltage (air gap induction) employing the proposed method and conventional *V/f* method.

increase in the rms current of about 20% is observed. However, the difference in the rms current decreases as the machine load increases, as shown in Table IV. For heavy machine loading (above 50%), the rms current with the third harmonic becomes lower than the rms current flowing when only the fundamental current is present. At 75% load, the proposed scheme produces an rms current 4% less than the conventional method, and at 100%,it produces 7% less rms current. This means that the rated torque can be produced with lower stator currents and about 14% lower stator winding losses. The torque/ampere ratio is also increased by about 7%.

Table IV also shows that the rms value of the induced voltage in the search coil increases with the inclusion of the third-harmonic current component; this increase being mainly due to the additional third-harmonic field produced in the air gap.

The practical results regarding the rotor speed at different load conditions show a speed increase when the developed control scheme is used, leading to a corresponding increase in the

mechanical power available on the shaft of about 4%. This increase in speed results in lower slip values and lower rotor currents. The reduction in the rotor current also results in lower losses in the rotor circuit. These facts allow to conclude that the use of a trapezoidal air gap induction can, in fact, increase the torque and power capability of the machine. The same torque is produced with lower currents and lower winding losses. The exact increase in the power capability is not trivial to state, as the change in the magnetic losses has not been considered here [17]. As shown in [18] and [19], a rectangular air gap induction changes the losses in the iron parts. Depending on the losses division between hysteresis and eddy current losses, the magnetic losses can be increased or decreased. In addition, the temperature rise in the machine has also to be accounted to establish the actual machine capability improvement. In order to have a deeper insight into the torque improvement, a test was undertaken allowing the load torque to increase until the stator current achieves the rated value (2.9 A). Under this condition, a torque of 3.10 Nm was measured. Therefore, assuming that the magnetic losses do not change and that the temperature rise does not exceed the value observed with the conventional *V/f* method, an increase in the torque capability of about 15% can be achieved under steady state. Under the same condition, an increase in the power capability of about 18% was observed when compared to the output power obtained for the same rms stator current using the conventional *V/f* method.

It is worthwhile to point out that despite the factors $\widehat{K}_{v1}$ and $\widehat{K}_{v3}$ having been adjusted to result in nearly trapezoidal induction at no load, their values assure practically the same air gap waveform even under load. This came from the fact that the terminal voltage was imposed by the inverter. On the other hand, the terminal voltage is balanced by the voltage induced by the resulting air gap field plus the voltage drop in the leakage reactance and the winding resistance. However, this voltage drop is much smaller than the air gap induced voltage and its influence can be disregarded. Hence, imposing the same terminal voltage under different load conditions practically imposes a constant induced voltage, and as a consequence, also imposes a constant air gap field. The currents, however, change to produce the necessary field.

To limit the scope of the paper, issues such as efficiency, power factor, and machine temperature rise have not been addressed in this paper, as they are complex issues making a fair comparison between control strategies including third-harmonic inclusion very difficult.

VI. Conclusion

This paper introduced a *V/f*-based control method for five-phase induction machines that generates a trapezoidal induction waveform in the air gap. This waveform best approximates the ideal waveform and is obtained by producing a third-harmonic induction component in the air gap. First, an optimal relationship between the fundamental and the third-harmonic induction components is determined, aiming to approximate a trapezoidal waveform. Using the machine steady-state model, an optimal relation for the applied voltage was determined and used to design the reference voltages. The proposed control scheme was simulated and applied to a prototype machine running under different load conditions. At steady state, the experimental results show that under light-load conditions (less than 50%), the conventional *V/f* method produces torque with lower rms current and lower stator losses. For load above 50%, the developed method performs better than the conventional method, as the same load torque is produced with lower stator and rotor currents. For the proposed control scheme, the rated torque is obtained with 7% less stator current and 14% less winding losses than the rated value. Furthermore, the rated torque is obtained with a lower slip, and thus, with lower rotor losses. If the stator rms current is allowed to increase up to the rated value and assuming that the magnetic losses do not change significantly, a torque increase of about 15% is obtained together with an increase of 18% in the output power. The torque increase comes from the additional torque produced by the third-harmonic current and induction component.

Acknowledgment

The authors would like to thank Prof. A. L. T. Ramos, Pontifícia Universidade Católica do Rio Grande do Sul (PUCRS) for his help in reviewing the text of this paper.

References

[1] A. Munoz-Garcia, T. A. Lipo, and D. W. Novotny, "A new induction motor *V/f* control method capable of high-performance regulation at low speeds," *IEEE Trans. Ind. Appl.*, vol. 34, no. 4, pp. 813–821, Jul./Aug. 1998.

[2] E. E. Ward and H. Harer, "Preliminary investigation of an inverter-fed 5-phase induction motor," *Proc. Inst. Elect. Eng.*, vol. 116, pp. 980–984, Oct. 1984.

[3] E. A. Klingshirn, "High phase order induction motors (Parts I and II)," *IEEE Trans. Power App. Syst.*, vol. PAS-102, no. 1, pp. 47–59, Jan. 1983.

[4] E. Levi, R. Bojoi, F. Profumo, and H. Toliyat, "Multiphase induction motor drives—A technology status review," *IET—Electric Power Appl.*, vol. 1, no. 4, pp. 489–516, 2007.

[5] H. A. Toliyat, "Analysis and simulation of five-phase variable-speed induction motor drives under asymmetrical connections," *IEEE Trans. Power Electron.*, vol. 13, no. 4, pp. 748–756, Jul. 1998.

[6] H. A. Toliyat, M. M. Rahimian, and T. A. Lipo, "dq modeling of five-phase synchronous reluctance machines including third harmonic of air gap mmf," in *Proc. IEEE Ind. Appl. Soc. Annu. Meet.*, Oct. 1991, pp. 231–237.

[7] P. De Silva, J. Fletcher, and B. Williams, "Design of a five-phase induction motor using flux distribution optimisation," *3rd IET Int. Conf. Power Electron., Mach. Drives*, 2006, pp. 331–335.

[8] J. Apsley, S. Williamson, A. Smith, and M. Barnes, "Induction motor performance as a function of phase number," *Proc. Inst. Elect. Eng.—Electr. Power Appl.*, vol. 153, no. 6, pp. 989–904, 2006.

[9] M. Duran, F. Barrero, S. Toral, and E. Levi, "Multi-dimensional space vector pulse width modulation scheme for five-phase series-connected two-motor drives," in *Electr. Mach. Drives Conf. IEMDC '07*, vol. 2, pp. 1208–1214.

[10] E. Levi, M. Jones, A. Iqbal, S. Vukosavic, and H. Toliyat, "Modeling, control, and experimental investigation of a five-phase series-connected two-motor drive with single inverter supply," *IEEE Trans. Ind. Electron.*, vol. 54, no. 3, pp. 1504–1516, Jun. 2007.

[11] H. A. Toliyat, T. Lipo, and J. C. White, "Analysis of a concentrated winding induction machine for adjustable speed drive applications (parts i and ii)," *IEEE Trans. Energy Convers.*, vol. 6, no. 4, pp. 679–692, Dec. 1991.

[12] R. Shi, H. Toliyat, and A. El-Antably, "Field oriented control of five-phase synchronous reluctance motor drive with flexible 3rd harmonic current injection for high specific torque," *36th IEEE Ind. Appl. Conf.*, 2001, pp. 2097–2103.

[13] H. Xu, H. Toliyat, and L. Petersen, "Five-phase induction motor drives with DSP-based control system," *IEEE Trans. Power Electron.*, vol. 17, no. 4, pp. 524–533, Jul. 2002.
[14] H. Xu, H. A. Toliyat, and L. J. Petersen, "Rotor field oriented control of five-phase induction motor with combined fundamental and third harmonic currents," in *Appl. Power Electron. Conf. Expo.—APEC 2001*, vol. 1, pp. 392–398.
[15] L. A. Pereira, C. C. Scharlau, L. F. A. Pereira, and J. F. Haffner, "General model of a five-phase induction machine allowing for harmonics in the air gap field," *IEEE Trans. Energy Convers.*, vol. 21, no. 4, pp. 891–899, Dec. 2006.
[16] D. C. White and H. H. Woodson, *Electromechanical Energy Conversion*. New York: Wiley, 1959.
[17] L. Dupré, M. Wulf, D. Makaveev, V. Permiakov, A. Pulnikov, and J. Melkebeek, "Modelling of electromagnetic losses in asynchronous machines," *COMPEL*, vol. 22, no. 4, pp. 1051–1065, 2004.
[18] L. Mthombeni and P. Pillay, "Core losses in motor laminations exposed to high-frequency or nonsinusoidal excitation," *IEEE Trans. Ind. Appl.*, vol. 40, no. 5, pp. 1325–1332, Oct. 2004.
[19] F. Fiorillo and A. Novikov, "An improved approach to power losses in magnetic laminations under nonsinusoidal induction waveform," *IEEE Trans. Magn.*, vol. 26, no. 5, pp. 2904–2910, Sep. 1990.

César Cataldo Scharlau received the B.E. degree in mechatronic engineering and the M.S. degree in electrical engineering from Pontifícia Universidade Católica do Rio Grande do Sul (PUCRS), Porto Alegre, Brazil, in 2002 and 2005, respectively.

He is currently professor at the Technology Faculty, National Industrial Training Service (SENAI), Porto Alegre. His current research interests include control of electrical machines and industrial automation.

Luís Fernando Alves Pereira received the B.E. degree in electrical engineering from Pontifícia Universidade Católica do Rio Grande do Sul (PUCRS), Porto Alegre, Brazil, in 1987, and the M.S. and Doctoral degrees from the Instituto Tecnológico de Aeronáutica (ITA), São José dos Campos, Brazil, in 1989 and 1995, respectively.

He is currently a Professor of electrical, control and computer engineering at PUCRS. His current research interests include the development of robust nonlinear control techniques applied on electric machines, power electronic devices, and mobile robots.

Luís Alberto Pereira received the B.E. degree in electrical engineering from Santa Maria Federal University, Santa Maria, Brazil, in 1986, the M.Sc. degree from Santa Catarina Federal University, Santa Catarina, Brazil, in 1992, and the Dr.-Ing. degree from the University of Kaiserslautern, Kaiserslautern, Germany, in 1997.

Since 1998, he has been a Professor of electrical engineering at Pontifical Catholic University of Rio Grande do Sul (PUCRS), Porto Alegre, Brazil. His current research interests include design and analysis of electrical machines and devices.

Sérgio Haffner (S'89–M'01) received the B.E. degree in electrical engineering from the Pontifical Catholic University of Rio Grande do Sul (PUCRS), Porto Alegre, Brazil, in 1987, and the M.S. and Dr. degrees in electrical engineering from State University of Campinas (UNICAMP), Campinas, Brazil, in 1990 and 2000, respectively.

Currently, he is an Associate Professor of Electrical Engineering in the Electrical Engineering Department of the State University of Santa Catarina (UDESC). His research interests include the power systems planning, operation, and optimization areas.